Mechanics of Materials 140 (2020) 103216

Contents lists available at ScienceDirect

Mechanics of Materials

journal homepage: www.elsevier.com/locate/mechmat

Research paper

The effect of loading duration on damage initiation in high-strength concrete

Colin Loeffler[a,*], Qiran Sun[a], William Heard[b], Bradley Martin[c], Brett Williams[a,b], Xu Nie[a]

[a] Southern Methodist University, Department of Mechanical Engineering, Dallas, TX, USA
[b] U.S. Army Engineer Research and Development Center, Vicksburg, MS 39180, USA
[c] Air Force Research Laboratory, Eglin AFB, FL 32542, USA

ARTICLE INFO

Keywords:
High-strength concrete
Kolsky bar
X-ray micro-CT
Damage
High strain-rate
Crack propagation

ABSTRACT

The rate sensitivity of the failure strength of concrete and other brittle materials is well documented. However, the underlying mechanism(s) that gives rise to this phenomenon remains a topic of debate. Experimental results suggest that the time-dependent failure process plays a significant role in the observed strength increase. This study investigates the failure process in high-strength concrete (HSC) specimens under uniaxial compression loading. This is accomplished through the use of a modified Kolsky compression bar to apply controlled and repeatable mechanical loading in combination with the non-destructive observation capability of high-resolution X-ray computed-microtomography (micro-CT). The evolution of specimen damage morphology is observed as a result of intermittent short-duration uniaxial stress loadings. Experimental results show that HSC specimens are capable of supporting the applied stress above their quasi-static failure strength for short durations. This duration is found to be a function of the overload stress level. Additionally, micro-CT results reveal that specimens undergo a brief period of void compaction followed by the coalescence and propagation of cracks before completely losing load bearing capability.

1. Introduction

The failure strength of HSC and other brittle materials has been widely reported to increase significantly as a function of strain rate (Bischoff and Perry, 1991; Heard et al., 2014; Malavar and Crawford, 1998; Ross et al., 1995). Experimental factors such as radial inertia, interfacial friction, and specimen size (Kim et al., 2010; Le Nard and Bailly, 2000; Li and Meng, 2003; Mu et al., 2012; Zhang et al., 2009) are often considered accountable for this strength increase. However, it has been shown that these effects can be significantly minimized through proper experimental design (Dai et al., 2010; Martin et al., 2018), which suggests that at least a portion of this strength increase is a result of the intrinsic material response.

The failure strength for brittle materials is typically obtained from monotonic constant strain-rate loading experiments, where the failure strength is taken to be the peak stress reached before the specimen loses load bearing capability (ASTM C39, 2016). Failure of brittle or quasi-brittle materials in uniaxial compression results from the nucleation of microcracks that propagate stably with increasing applied load. The continued growth and coalescence of these microcracks leads to the onset of unstable crack growth followed by spontaneous and rapid specimen collapse (Horii and Nemat-Nasser, 1985; Shah et al., 1995). In a typical quasi-static experiment, the slow loading rate in conjunction with the rapid unstable crack growth results in a negligible stress increase between the onset of strain localization and complete specimen collapse. This is especially true for higher-strength and ultra-high-strength concretes, such as the material studied here, which exhibit a more brittle response when compared to conventional concrete. Conversely, in a typical dynamic loading experiment the rate of deformation is as much as six orders of magnitude higher. In this case, the time-dependent nature of the failure process may result in a significant stress increase between the onset of failure processes and specimen collapse. Therefore, a complete understanding of the entire failure process, especially under dynamic loading conditions, is beneficial for the development of more accurate constitutive models for brittle materials.

Experimental studies of brittle solids under high-strain-rate compression have demonstrated the significant stress increase that can occur after the onset of unstable crack growth (Janach, 1976; Jiao et al., 2004; Nie et al., 2007). These results suggest that a significant portion of the observed strength increase is a result of the structural response of the specimen after the onset of major crack propagation. Additionally, numerical studies have been performed to investigate the dynamic

* Corresponding author.
E-mail address: cloeffler@smu.edu (C. Loeffler).

https://doi.org/10.1016/j.mechmat.2019.103216
Received 30 April 2019; Received in revised form 17 October 2019; Accepted 17 October 2019
Available online 18 October 2019
0167-6636/ © 2019 Elsevier Ltd. All rights reserved.

failure process in concretes. However, they often treat the material as a continuum and therefore do not explicitly model the effects of porosity and aggregates. Numerical studies that do explicitly model the effects of porosity have found that the size and distribution of voids have a significant role in the rate-dependent failure observed in brittle materials (Katcoff and Graham-Brady, 2014; Snozzi et al., 2012). Unfortunately, there is very limited experimental work on the interaction of damage evolution with the internal void structure in concrete especially under dynamic loading.

While the apparent strength increase under high-rate loading is likely due to some combination of experimental factors, structural effects, and the inherent material behavior, it is evident that the failure process in brittle materials plays a significant role in the observed rate sensitivity. This study aims to investigate the entire failure process in high-strength concretes under dynamic uniaxial compression in order to gain a deeper understanding of its effects on the observed strength enhancement. This is accomplished using a high-resolution desktop micro-CT scanner, which provides 3D images of the internal specimen morphology with high spatial resolution. Micro-CT imaging is coupled with an in-house developed damage segregation algorithm and a modified Split Hopkinson (Kolsky) Compression Bar to apply controlled and repeatable mechanical loading. These capabilities enable the observation of crack initiation and propagation as well as the evolution of pre-existing voids as a result of dynamic intermittent loading.

2. Experimental procedure

2.1. Material and specimen preparation

The material used in this study is a self-consolidating high-strength concrete developed by the U.S. Army Engineer Research and Development Center (ERDC)(Heard, 2014). Cylinders of 18.25 mm diameter were core drilled from the bulk material and then cut into individual specimens roughly 19 mm long. Each specimen was then carefully brought to its final length of 12.7 mm in a two-step process involving a precision surface grinder and finally a double-sided planetary lapping machine. This procedure maximizes the flatness and parallelism of the specimen ends within 25 μm in order to minimize stress concentrations at the bar/specimen interfaces during dynamic loading. This relatively small specimen geometry can be considered representative of the bulk material due to the small aggregate size (< 3 mm) (Bischoff and Perry, 1991; Cadoni et al., 2009; Caverzan et al., 2016). A cross section of a typical specimen, obtained using X-ray micro-CT, is shown in Fig. 1(a). Additionally, this specimen geometry allows the use of smaller diameter Kolsky compression bars and facilitates higher resolution micro-CT scans. As shown in Fig. 1(b), the effects of specimen size and strain rate on the failure strength of this material have been characterized in a previous study (Martin et al., 2018). In general, the average peak failure strength for this material using this specimen geometry increased from 110 MPa at 1 e^{-4}/s to 200 MPa at 200/s.

2.2. Dynamic loading mechanism

During a conventional high-strain-rate loading experiment on concrete, specimens are deformed at a constant strain rate until complete loss of load bearing capability. This means that not only are specimens subjected to an elevated strain rate, but consequently, the applied stress is rapidly increasing throughout the loading process. The combination of increasing applied stress and the high deformation rate complicates speculation on their influence on the observed specimen behavior. In an attempt to delineate the effects of applied stress level from those of strain rate, impulse loading waves were specially designed such that specimens were subjected to a short duration (< 300 μs) constant uniaxial compression at pre-determined stress levels. Holding the applied stress constant allows the effects of applied stress to be studied independent from those of strain rate. This is achieved using a Kolsky Compression Bar system with single loading capability. The Kolsky bar is a well-known and established experimental technique to impose high-strain-rate deformation on specimens made from different materials through a wave tailoring technique called pulse shaping (Chen and Song, 2011). The Kolsky compression bar implemented in this study consists of a 3.65 m (12 ft) long incident bar and 1.82 m (6 ft) transmission bar both 19 mm in diameter and comprised of maraging C300 steel alloy. The striker bar used for all experiments presented here is made from the same material with the same diameter and 762 mm (2.5 ft) in length. The system utilizes a compressed air gun with a barrel 1.82 m (6 ft) in length to accelerate the striker bar to the desired velocity. Stress waves are recorded as they propagate along the bars using pairs of strain gages adhered to the incident and transmission bar surfaces. The strain gage pairs are connected to a Wheatstone bridge circuit with the output voltage recorded by a high-resolution digital oscilloscope. The pulse shapers used for this study were annealed copper disks approximately 0.27 mm thick with diameters ranging from 3 mm to 5.5 mm.

The amplitudes of the constant stress loading pulses were selected to be at various levels above the quasi-static failure strength of the HSC material. The application of this overload ensures the initiation of damage, while the use of the Kolsky bar enables measurement of the specimen's mechanical response with high temporal resolution under

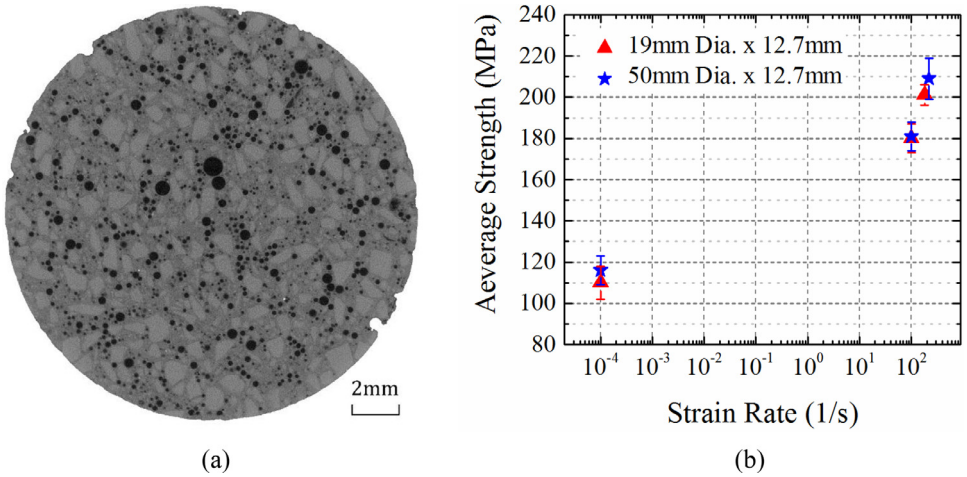

Fig. 1. Representative micro-CT cross-sectional slice of an HSC specimen (a) and the failure stress as a function of strain rate for three different specimen geometries in unconfined uniaxial compression (Martin et al., 2018) (b).

short loading durations. Furthermore, this experimental design allows the loading duration to be adjusted such that the specimen can be unloaded after the initiation of damage but before complete fragmentation. Similar to the methodology of Huang et al. (2013) and Wu et al. (2014) this experimental design facilitates detailed analysis of the partially damaged specimens in between dynamic loading events. The analysis after each loading cycle can include visual inspection, X-ray analysis, and measurement of mechanical properties. However, the experimental design proposed by Huang et al. and Wu et al. control the strain rate of deformation by tailoring of the incident loading wave and employed a displacement control technique to limit the maximum deformation and ensure unloading of the specimen before complete failure occurs. Whereas in this study unloading prior to failure is achieved by limiting the duration and amplitude of the applied loading. Results of micro-CT scans taken before and after each loading are then compared to a scan of the pristine specimen taken before loading to investigate changes in the specimen morphology as a result of the applied loading history.

2.3. Micro-CT analysis

The micro-CT scans in this study were obtained using a Bruker SkyScan 1172 high-resolution desktop micro-CT scanner. This scanner provides a spatial resolution of 5.24 μm for a specimen geometry of 18.25 mm diameter by 12.7 mm thick with a total volume of 4000 × 4000 × 2300 voxels. For each of the scans used in this study, the acceleration voltage was set to 100 kV with copper and aluminum filters used to filter out low energy X-Rays. During each scan, the specimen was rotated a total of 360° with a step size of 0.15° resulting in 2400 projection images. The projection images were then used to reconstruct a 3D tomography of the specimen with commercial software utilizing the Feldkamp cone-beam algorithm. Following each reconstruction, the images are registered to the original scan of the undamaged specimen to improve analysis of the specimen morphology evolution.

The heterogeneous nature of the concrete material complicates analysis of the specimen morphology in the reconstructed micro-CT images. The various constitutive components in the specimen volume can be identified and separated using conventional grayscale segmentation methods. However, grayscale segmentation methods alone are inadequate to separate loading induced cracks from pre-existing porosity. The identification of loading induced cracks can be accomplished through the use of geometric segmentation methods (Loeffler et al., 2018; Nagy et al., 2001). The implementation of geometric segmentation methods allows the pre-existing porosity and loading-induced cracks to be analyzed separately. This capability, when coupled with the controlled Kolsky bar dynamic loading technique, facilitates the analysis of specimen morphology (especially damage) evolution as a result of the repeated constant stress loading.

3. Results and discussions

3.1. Stress–Strain response

The stress, strain, and strain-rate histories recorded for a single HSC specimen subjected to a constant uniaxial stress loading pulse of ~140 MPa are presented in Fig. 2. When the stress is first applied, there is an initial rapid increase in strain-rate as the specimen deforms under the applied load.

As the stress level plateaus, the strain rate steadily decreases to near zero after approximately 150 μs. This trend is also reflected in the strain history which shows a saturation after initial rise. Throughout this duration, the specimen is supporting a load well above its quasi-static failure strength with little deformation. The end of this constant stress loading is marked by an increase in the strain-rate corresponding to an exponential increase in specimen strain and a decrease in specimen stress. This increase in strain-rate is caused by a significant decrease in the specimen stiffness caused by the coalescence of one or more major cracks and strain localization (Shah et al., 1995).

Experiments of this type were repeated many times and exhibited results similar to the behavior displayed in Fig. 2. To investigate the time duration for which specimens could support the applied overload, the stress level applied to each specimen was varied. The results from these experiments are presented in Fig. 3 in the form of a scatterplot. This figure clearly exhibits a correlation between the applied stress level and its respective loading duration prior to specimen failure. Applying an exponential decay fit to these data reveals a trend that asymptotically approaches the average quasi-static strength for these specimens as the loading duration increases. The results also demonstrate that this stress threshold appears to occur after approximately 400 μs of loading. Since a typical quasi-static test normally takes several seconds to several minutes, these findings may shed light on the early development of damage in concrete that leads to catastrophic failure at the peak stress. Additionally, the total duration to failure found in these experiments is significant when compared to the duration of a typical high-strain-rate experiment (200–300 μs). Fig. 3 also implies that the total loading duration required to initiate damage in the material decreases with increasing stress level. In dynamic constant strain-rate experiments where the specimens experience a monotonic stress increase, the damage initiation is likely dependent on the competition between the rising stress and the consequent decrease of loading duration. These experimental findings may provide a new perspective in explaining the widely observed strain-rate effects of concrete failure strength especially under dynamic loading conditions.

There are two limitations in the current constant stress experiments that must be mentioned here. First, due to the nature of the Kolsky bar apparatus, the constant stress cannot be applied instantaneously, and therefore, the amount of time required to ramp up the applied stress must be considered. For lower amplitude loadings, this duration is significantly shorter than the constant stress duration, and therefore renders limited impact to the data interpretation. However, as the stress amplitude is increased, this duration becomes more significant. This is why constant stress durations less than ~50 μs are difficult to achieve without accounting for a substantial stress buildup process above the quasi-static failure strength. Secondly, due to the limited length of the Kolsky bar apparatus used in this study, the duration of the longest possible constant stress pulse is approximately 300 μs. In this case, multiple loading cycles are required to achieve longer loading durations. These additional loading and unloading cycles may affect the overall specimen response. To investigate the effect of these additional loading cycles, an input loading wave was designed to mimic only the loading/unloading trails without the constant stress plateau in between. Specimens subjected to this loading arrangement required significantly more loading cycles (at least 20–100 depending on stress levels) before damage occurred. Considering that even the longest loading duration imposed on the specimens presented in Fig. 3 (~1100 μs) at the lowest stress level comprises only 5–6 loading cycles, it is reasonable to assume that the specimens' responses are dominated by the constant stress portions of the loading history. Despite the aforementioned limitations, the use of multiple loading cycles has the benefit of allowing detailed micro-CT analysis of the recovered specimens in between each loading cycle.

3.2. Response of an individual specimen

Fig. 4 shows the results obtained from a single HSC specimen subjected to repeated constant stress loading pulses with ~126 MPa amplitude and 300 μs duration. A total of six (6) loading cycles are presented in this figure to demonstrate the excellent repeatability of these tests. As shown in Fig. 4, the specimen completely fractured during the 6th loading cycle causing the transmitted wave to drop.

Micro-CT scans were taken before and after each loading cycle to

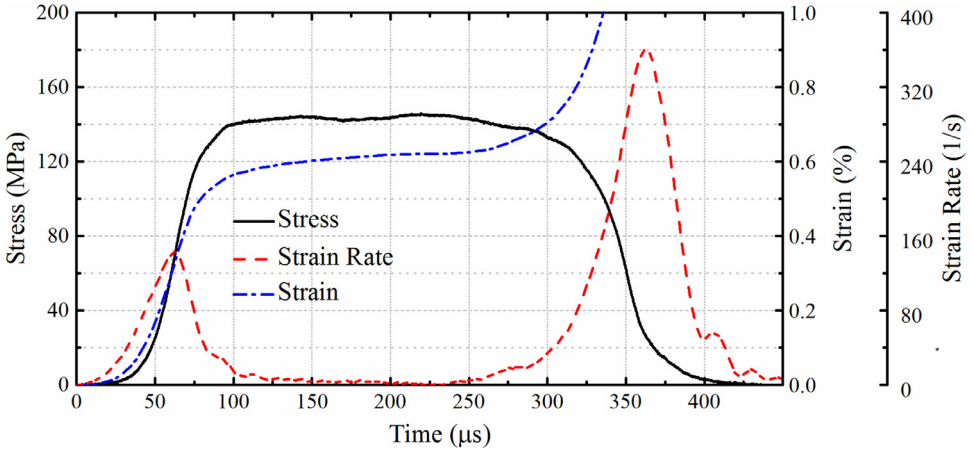

Fig. 2. Stress, Strain, and Strain-rate histories of a single HSC specimen subjected to a uniaxial compressive stress of approximately 140 MPa.

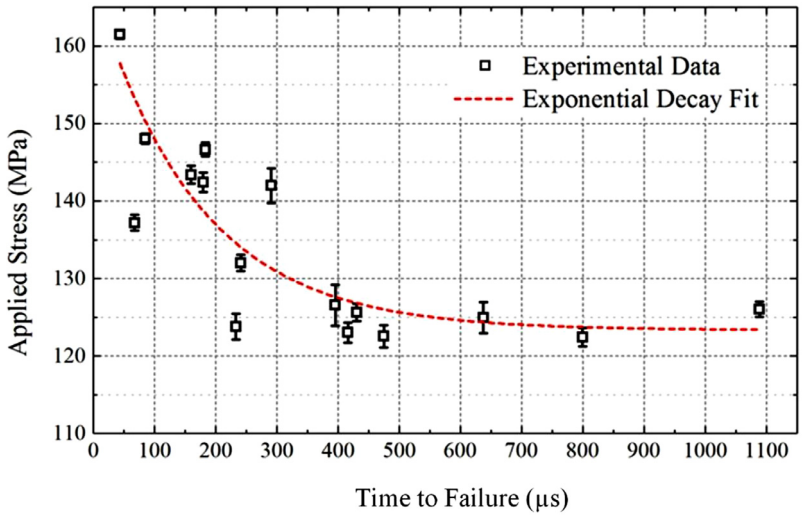

Fig. 3. Experimental characterization of the relation between the applied constant stress and total loading duration to failure for concrete specimens.

monitor the changes in microstructure with particular attention to the damage initiation and evolution. The specimen was loaded and recovered five times before complete failure occurred approximately 100 μs into the sixth and final loading cycle. This allowed a total of six micro-CT scans to be conducted throughout the loading process including an initial scan taken of the pristine specimen. Fig. 5 shows the same cross sectional slice from the micro-CT scans taken after the 4th and 5th loading cycles with the detected cracks magnified and highlighted. Loading induced cracks were not detected until after the 4th loading cycle as shown in Fig. 5(a). This crack network was observed to have grown after the 5th loading cycle, as shown in Fig. 5(b), and led to complete specimen collapse in the 6th and final loading cycle. The crack network shown in Fig. 5 indicates that the onset of strain localization occurred during the 4th loading cycle. However crack growth ceased when the applied load was removed, indicating that the crack propagation remained stable until the 6th loading cycle. As shown in Fig. 5, the crack network initiated near the periphery of the specimen, this trend was consistently observed in recovered specimens and is likely due to the slight (and inevitable) stress concentration resulting from the specimen/bar contact surface.

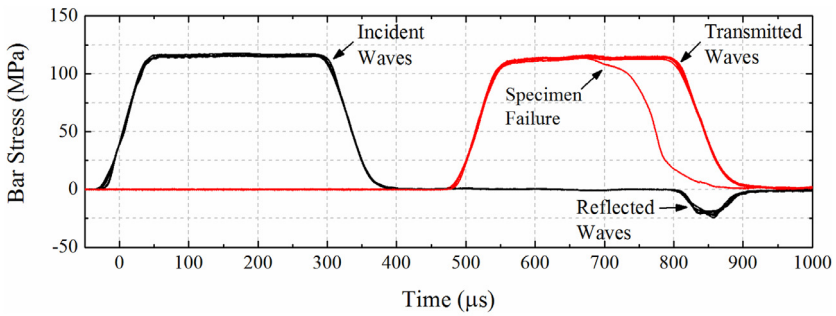

Fig. 4. The six incident, reflected, and transmitted waves recorded during the loading of a single HSC specimen. Specimen failure took place during the 6th loading cycle.

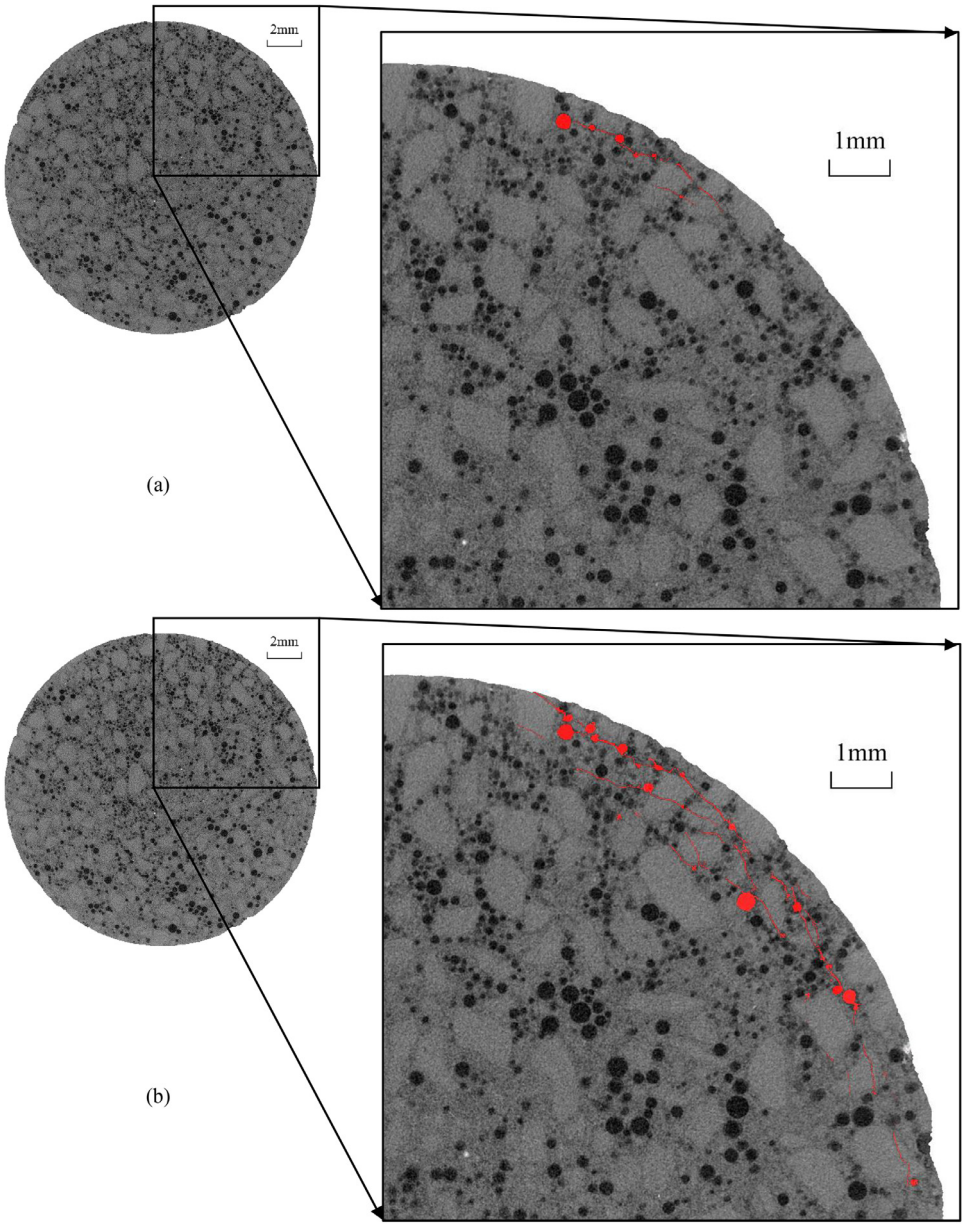

Fig. 5. Tomography of the same slice in the concrete specimen taken after (a) the 4th loading cycle and (b) the 5th loading cycle, with the crack network magnified and highlighted in red. (For interpretation of the references to color in this figure legend, the reader is referred to the web version of this article.)

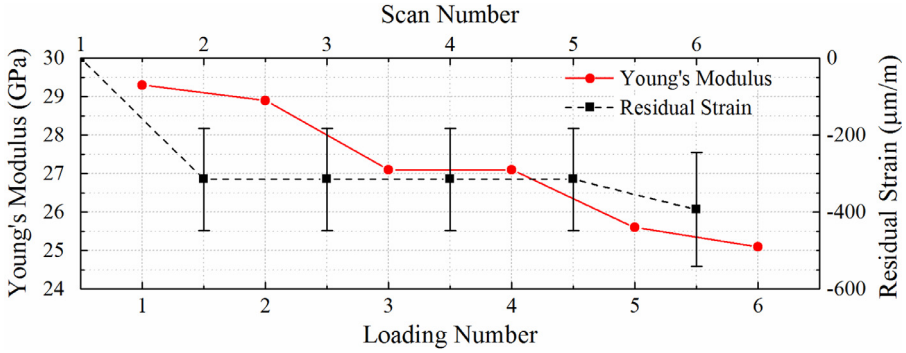

Fig. 6. The residual strain and stiffness for the HSC specimen subjected to 6 short-duration, constant-stress, loading cycles.

Measurements taken of the recovered specimen using a high-resolution digital micrometer revealed a slight accumulation of residual strain after the 1st and 5th loading cycles. Additionally, a slight decrease in specimen stiffness was observed during each loading cycle. These observed trends are plotted in Fig. 6. It must be noted that while the strain accumulation was measurable, the total change in specimen

length was on the order of 4 μm which is near the least count of the measurement device, resulting in the relatively large error bars shown in Fig. 6.

The observed decrease in specimen stiffness is believed to be caused by the initiation and propagation of microcracks with apertures below the micro-CT resolution. However, during the 4th loading cycle, these micro-cracks coalesced to form a crack network large enough to be detected in the 5th micro-CT scan. This crack network is believed to be the primary cause of the decrease in specimen stiffness observed in the final two loading cycles. A portion of this crack network and its evolution during the 5th loading cycle is shown in Fig. 5b, where the same cross-sectional slice of the specimen in scans 5 and 6 are displayed with the crack network highlighted and magnified. The maximum crack aperture (excluding connected porosity) in scan 6 was found to be 36.7 μm (7 pixels).

In order to gain a deeper understanding of the observed mechanical response, a detailed analysis of the micro-CT scans obtained before and after each loading cycle was conducted. The micro-CT data obtained in between each loading cycle offered an excellent opportunity to study the changes in specimen morphology as a result of the mechanical loading in a more quantitative fashion. A connected components algorithm allows each individual cavity in the micro-CT scans to be identified, labeled, and measured. This procedure allows tracking of an individual void or a subset of voids through each scan to observe its evolution as a result of the intermittent mechanical loading. Additionally, by using the procedure outlined in Loeffler et al. (2018), preexisting voids in the micro-CT scans can be differentiated from loading-induced cracks in order to investigate their evolution independently.

A preliminary analysis of the micro-CT results revealed a small but measurable decrease in the overall specimen porosity after the first 3 loading cycles (scans 2–4) as shown in Fig. 7. This decrease is followed by an increase in porosity observed in the fifth and sixth scans corresponding to the coalescence and growth of a crack network. Analysis of the void distribution revealed no significant decrease in the number of voids, meaning the decrease in porosity is not a result of void collapse. To further investigate this observed porosity decrease before the initiation of major crack propagation, a representative subset of voids was selected for geometric analysis. This subset is selected to include all voids that did not become connected to the crack network in the fifth and sixth scans, allowing the influence of the crack network on the porosity analysis to be eliminated. Additionally, the subset also excluded voids smaller than approximately 6 voxels in diameter, as the error in geometric measurements due to the partial volume effect (Herman, 2009) is more significant for smaller volumes. The equivalent diameter of each void in this subset is calculated, and the average equivalent diameter of the subset is also plotted in Fig. 7.

These results indicate that the observed decrease in overall porosity prior to damage initiation is due to void compaction. Tracking the evolution of a subset of voids separated from the crack network also revealed that this trend continues after the initiation of major crack propagation. A significant decrease in the average void diameter is observed between the final two scans just before the complete failure of the specimen. This is likely caused by the loss of load bearing capacity in the region of the specimen affected by the crack network, which results in a redistribution of stress to the intact portions of the specimen and therefore increased void compaction. Further analysis of void-shape measurements did not reveal any preferential directionality in the void size decrease. While void dimensions may be expected to decrease primarily along the direction of the loading axis, the micro-CT analysis does not suggest any anisotropy in void compaction. However, it needs to be pointed out that the detected average diameter change is only slightly higher than the spatial resolution of the CT scans. The lack of observed anisotropy can be affected by this experimental constraint. Future analysis with higher resolution CT scans may shed more light on the evolution of porosity in concrete under dynamic loading conditions.

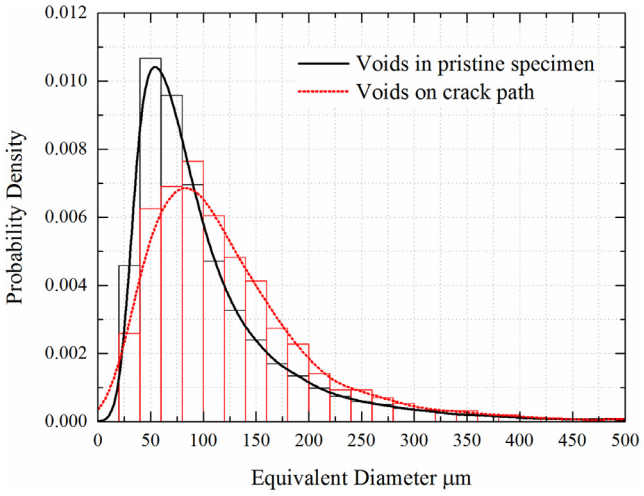

Fig. 8. Comparison of void diameter distribution between the pristine specimen and the subset that eventually became connected to the crack network.

An additional analysis of the voids subset that did eventually become connected to the crack network was also performed. The distribution of void size in the pristine specimen and the subset of voids that lay on the crack path are compared in Fig. 8. As shown in this figure, there is a notable difference in size distribution between these two groups of voids. The two plots cross over at around 90 μm equivalent void diameter. The evolving crack network appears to have a clear preference to interact with larger size voids in the bulk, possibly due to the higher splitting tensile stress that occurs around larger voids. This indicates that crack propagation in concrete materials can be influenced by specific microstructural features, and a preferential crack propagation path might exist for concrete materials with inhomogeneous void size distribution. These results agree with some

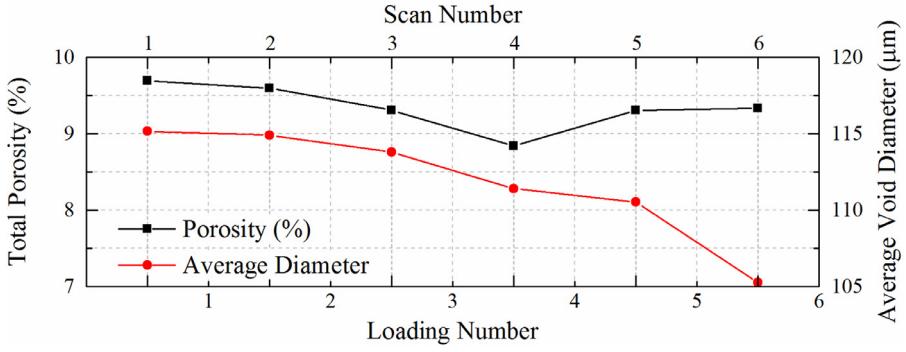

Fig. 7. The total porosity and the average equivalent diameter of a representative subset of voids measured in each micro-CT scan.

previously published studies which found that, at lower strain-rates, cracks tend to nucleate from larger flaws (Horii and Nemat-Nasser, 1986; Li et al., 2013; Wong et al., 2006). These experimental findings may provide important underpinning for multi-scale damage model development and validation, which will hopefully provide more insight into the damage evolution process in high-performance concrete materials under dynamic loadings.

4. Summary

In this study, the mechanical response of HSC specimens subjected to short duration constant stress loadings was carefully analyzed. The experimental results show that under uniaxial compressive loading, HSC specimens were capable of supporting mechanical stress above their failure strength for short durations. The duration for which HSC specimens are capable of supporting an applied overload was found to be highly dependent on the applied stress. This discovery may have important implications on the widely observed strain-rate effects of concrete failure strength. The morphological evolution of a single HSC specimen subjected to six constant stress loading cycles was carefully analyzed. A slight accumulation of permanent strain accompanied by a decrease in specimen stiffness as a result of the applied loading was observed. Micro-CT analysis of the specimens performed in between each loading cycle revealed a decrease in porosity caused by void compaction before the coalescence of a major crack network. These results show that the failure process in HSC specimens is comprised of a period of void compaction, likely accompanied by the propagation of microcracks, followed by the coalescence and propagation of major cracks as well as continued void compaction. The time-dependent nature of these processes suggest that they may have a significant influence on the dynamic failure process in HSC. Finally, analysis of the voids that lay in the crack path suggests that the cracks preferentially propagate through larger voids in the specimen. Experimental techniques developed in this study may be employed to further investigate the effect of constant high-strain-rate loading on the failure initiation and evolution of HSC materials.

Declaration of Competing Interest

The authors declare that they have no known competing financial interests or personal relationships that could have appeared to influence the work reported in this paper.

Acknowledgments

Dr. Xu Nie gratefully acknowledges financial support from the U.S. Air Force Research Laboratory (AFRL) under agreement number FA8651-14-2-0007, and the U.S. Army Engineer Research and Development Center (ERDC) under contract number W912HZ-14-C-0021. Permission to publish was granted by the Directors of the AFRL Munitions Directorate, case number 96TW-2018-0017, and the ERDC Geotechnical and Structures Laboratory.

Supplementary materials

Supplementary material associated with this article can be found, in the online version, at doi:10.1016/j.mechmat.2019.103216.

References

ASTM C39, 2016. Standard test method for compressive strength of cylindrical concrete specimens. Am. Soc. Test. Mater. https://doi.org/10.1520/C0039.
Bischoff, P.H., Perry, S.H., 1991. Compressive behaviour of concrete at high strain rates. Mater. Struct. 24, 425–450. https://doi.org/10.1007/BF02472016.
Cadoni, E., Solomos, G., Albertini, C., 2009. Mechanical characterisation of concrete in tension and compression at high strain rate using a modified Hopkinson bar. Mag. Concr. Res. 61, 221–230. https://doi.org/10.1680/macr.2006.00035.
Caverzan, A., Peroni, M., Solomos, G., 2016. Compressive behaviour of dam concrete at higher strain rates. Eur. Phys. J. Spec. Top. 225, 283–293. https://doi.org/10.1140/epjst/e2016-02628-5.
Chen, W., Song, B., 2011. Split Hopkinson (Kolsky) Bar. Split Hopkinson (Kolsky) Bar, first ed. Springer US, Boston, MA. https://doi.org/10.1007/978-1-4419-7982-7.
Dai, F., Huang, S., Xia, K., Tan, Z., 2010. Some fundamental issues in dynamic compression and tension tests of rocks using split Hopkinson pressure bar. Rock Mech. Rock Eng. 43, 657–666. https://doi.org/10.1007/s00603-010-0091-8.
Heard, W.F., 2014. Development and Multi-Scale Characterization of a Self-Consolidating High-Strength Concrete for Quasi-Static and Transient Loads. Vanderbilt University.
Heard, W.F., Martin, B.E., Nie, X., Slawson, T., Basu, P.K., 2014. Annular pulse shaping technique for large-diameter Kolsky bar experiments on concrete. Exp. Mech. 54, 1343–1354. https://doi.org/10.1007/s11340-014-9899-6.
Herman, G.T., 2009. Fundamentals of Computerized Tomography, Scientific American, Advances in Pattern Recognition. Springer London, London. https://doi.org/10.1007/978-1-84628-723-7.
Horii, H., Nemat-Nasser, S., 1986. Brittle failure in compression: splitting, faulting and brittle-ductile transition. Philos. Trans. R. Soc. London Ser. A Math. Phys. Sci. 319, 337–374. https://doi.org/10.1098/rsta.1986.0101.
Horii, H., Nemat-Nasser, S., 1985. Compression-induced microcrack growth in brittle solids: axial splitting and shear failure. J. Geophys. Res. 90, 3105–3125. https://doi.org/10.1029/JB090iB04p03105.
Huang, S., Xia, K., Zheng, H., 2013. Observation of microscopic damage accumulation in brittle solids subjected to dynamic compressive loading. Rev. Sci. Instrum. 84, 093903. https://doi.org/10.1063/1.4821497.
Janach, W., 1976. The role of bulking in brittle failure of rocks under rapid compression. Int. J. Rock Mech. Min. Sci. Geomech. Abstr. 13, 177–186. https://doi.org/10.1016/0148-9062(76)91284-5.
Jiao, T., Li, Y., Ramesh, K.T., Wereszczat, A.A., 2004. High rate response and dynamic failure of structural ceramics. Int. J. Appl. Ceram. Technol. 1, 243–253. https://doi.org/10.1111/j.1744-7402.2004.tb00176.x.
Katcoff, C.Z., Graham-Brady, L.L., 2014. Modeling dynamic brittle behavior of materials with circular flaws or pores. Int. J. Solids Struct. 51, 754–766. https://doi.org/10.1016/j.ijsolstr.2013.11.004.
Kim, D., Sirijaroonchai, K., El-Tawil, S., Naaman, A.E., 2010. Numerical simulation of the split Hopkinson pressure bar test technique for concrete under compression. Int. J. Impact Eng. 37, 141–149. https://doi.org/10.1016/j.ijimpeng.2009.06.012.
Le Nard, H., Bailly, P., 2000. Dynamic behaviour of concrete: the structural effects on compressive strength increase. Mech. Cohesive-Frictional Mater. 5, 491–510. https://doi.org/10.1002/1099-1484(200008)5:6<491::AID-CFM106>3.0.CO;2-R.
Li, J., Huang, Q., Ren, X., 2013. Dynamic initiation and propagation of multiple cracks in brittle materials. Materials (Basel) 6, 3241–3253. https://doi.org/10.3390/ma6083241.
Li, Q.M., Meng, H., 2003. About the dynamic strength enhancement of concrete-like materials in a split Hopkinson pressure bar test. Int. J. Solids Struct. 40, 343–360. https://doi.org/10.1016/S0020-7683(02)00526-7.
Loeffler, C.M., Qiu, Y., Martin, B., Heard, W., Williams, B., Nie, X., 2018. Detection and segmentation of mechanical damage in concrete with X-Ray microtomography. Mater. Charact. 142, 515–522. https://doi.org/10.1016/j.matchar.2018.06.018.
Malavar, L.J., Crawford, J.E., 1998. Dynamic increase factors for concrete. In: Twenty-Eighth DDESB Seminar. Orlando, FL. pp. 1–17.
Martin, B.E., Heard, W.F., Loeffler, C.M., Nie, X., 2018. Specimen size and strain rate effects on the compressive behavior of concrete. Exp. Mech. 58, 357–368. https://doi.org/10.1007/s11340-017-0355-2.
Mu, Z.C., Dancygier, A.N., Zhang, W., Yankelevsky, D.Z., 2012. Revisiting the dynamic compressive behavior of concrete-like materials. Int. J. Impact Eng. 49, 91–102. https://doi.org/10.1016/j.ijimpeng.2012.05.002.
Nagy, G., Zhang, T., Franklin, W.R., Landis, E., Nagy, E., Keane, D.T., 2001. Volume and surface area distributions of cracks in concrete. Visual Form 2001. Lecture Notes in Computer Science. pp. 759–768. https://doi.org/10.1007/3-540-45129-3_70.
Nie, X., Chen, W.W., Sun, X., Templeton, D.W., 2007. Dynamic failure of borosilicate glass under compression/shear loading experiments. J. Am. Ceram. Soc. 90, 2556–2562. https://doi.org/10.1111/j.1551-2916.2007.01819.x.
Ross, A., Tedesco, J.W., Kuennen, S.T., 1995. Effects of strain rate on concrete strength. ACI Mater. J. 92, 37–43.
Shah, S.P., Swartz, S.E., Ouyang, C., 1995. Fracture Mechanics of Concrete : Applications of Fracture Mechanics to Concrete, Rock, and Other Quasi-Brittle Materials. John Wiley & Sons, Inc., New York.
Snozzi, L., Gatuingt, F., Molinari, J.F., 2012. A meso-mechanical model for concrete under dynamic tensile and compressive loading. Int. J. Fract. 178, 179–194. https://doi.org/10.1007/s10704-012-9778-z.
Wong, R.H.C., Lin, P., Tang, C.A., 2006. Experimental and numerical study on splitting failure of brittle solids containing single pore under uniaxial compression. Mech. Mater. 38, 142–159. https://doi.org/10.1016/j.mechmat.2005.05.017.
Wu, B., Kanopoulos, P., Luo, X., Xia, K., 2014. An experimental method to quantify the impact fatigue behavior of rocks. Meas. Sci. Technol. 25. https://doi.org/10.1088/0957-0233/25/7/075002.
Zhang, M., Wu, H.J., Li, Q.M., Huang, F.L., 2009. Further investigation on the dynamic compressive strength enhancement of concrete-like materials based on split Hopkinson pressure bar tests. Part I: experiments. Int. J. Impact Eng. 36, 1335–1345. https://doi.org/10.1016/j.ijimpeng.2009.04.009.